JOM, Vol. 67, No. 10, 2015
DOI: 10.1007/s11837-015-1590-6

Trace Carbon in Biomedical Beta-Titanium Alloys: Recent Progress

D. ZHAO,[1] T. EBEL,[2] M. YAN,[3,5] and M. QIAN[4,6]

1.—College of Biology, Hunan University, Changsha 410082, People's Republic of China. 2.—Helmholtz-Zentrum Geesthacht, Institute of Materials Research, 21502 Geesthacht, Germany. 3.—Department of Materials Science and Engineering, South University of Science and Technology of China, 518055 Shenzhen, People's Republic of China. 4.—School of Aerospace, Mechanical and Manufacturing Engineering, Centre for Additive Manufacturing, RMIT University, Melbourne, VIC 3000, Australia. 5.—e-mail: yanm@sustc.edu.cn. 6.—e-mail: ma.qian@rmit.edu.au

Owing to their relatively low Young's modulus, high strength, good resistance to corrosion, and excellent biocompatibility, β-titanium (Ti) alloys have shown great potential for biomedical applications. In β-Ti alloys, carbon can exist in the form of titanium carbide (TiC_x) as well as interstitial atoms. The Ti-C binary phase diagram predicts a carbon solubility value of 0.08 wt.% in β-Ti, which has been used as the carbon limit for a variety of β-Ti alloys. However, noticeable grain boundary TiC_x particles have been observed in β-Ti alloys containing impurity levels of carbon well below the predicted 0.08 wt.%. This review focuses its attention on trace carbon (≤0.08 wt.%) in biomedical β-Ti alloys containing niobium (Nb) and molybdenum (Mo), and it discusses the nature and precipitation mechanism of the TiC_x particles in these alloys.

INTRODUCTION

New generation aluminum (Al)- and vanadium (V)-free, biomedical β-Ti alloys are being widely pursued for at least two good reasons:

1. The Al and V elements in the Ti-6Al-4V alloy are found to be associated with some long-term health problems, most notably Alzheimer disease, neuropathy, and osteomalacia due to the release of Al and V ions to human body.
2. They offer lower Young's modulus than Ti (~100 GPa) and Ti-6Al-4V (~110 GPa); in particular some β-Ti alloys can have Young's modulus close to human bones' (~30 GPa).[1–3] This helps to mitigate the so-called "stress-shield" impact arising from the mismatch in modulus between the implant material and human bone.

When further compared with CP-Ti, β-Ti alloys generally show higher strength and hardness, making them more suitable for applications such as bone screws, plates, and similar products.[3] As a result, a variety of biomedical β-Ti alloys, for example, Ti-35Nb-5Ta-7Zr-0.4O and Ti-15Mo, have been developed during the last two decades.[4,5] It is noted that many such biomedical β-Ti alloys contain a significant level of Nb and/or Mo (β-stabilizers), assisted with the addition of a few other elements including Zr and Sn, which are neutral elements to Ti.[6–10]

Impurity elements (e.g., O, N, H, and Fe) can noticeably affect the microstructure and/or mechanical properties of Ti and Ti alloys. For example, a small increase in oxygen content (from 0.25 wt.% to 0.33 wt.%) can reduce the ductility of Ti-6Al-4V from 15% to 8%, which occurs similarly to a biomedical β-Ti alloy, i.e., Ti-29Nb-13Ta-4.6Zr.[11,12] Besides, the presence of 0.3 wt.% Fe can significantly refine the β-Ti grains in Grade 7 Ti.[13] However, compared with O, Fe, N, and H, the role of trace carbon (C) in β-Ti alloys has not received adequate attention as yet, especially in biomedical β-Ti alloys. Table I lists the carbon limits for several important near β- and β-Ti alloys, two commercial biomedical β-Ti alloys, Grade 1 commercially pure Ti (CP-Ti), and Ti-6Al-4V. The carbon limits are set as either (0.08–0.10) wt.% or 0.05 wt.% in order to avoid carbide formation. In fact, this is also the case for most other Ti materials including other β-Ti alloys. The underlying reason can be inferred from Fig. 1, the Ti-C binary phase diagram up to

(Published online August 28, 2015)

Table I. Impurity specifications for grade 1 CP-Ti and some selected Ti alloys[15,22,39]

Composition	N max.	C max.	H max.	Fe max.	O max.	Standard
Grade 1 (CP-Ti)	0.03	0.08	0.015	0.20	0.18	ASTM F67
Grade 5 (Ti-6Al-4V)	0.05	0.08	0.015	0.40	0.20	ASTM B348
Ti-10V-2Fe-3Al	0.05	0.05	0.015	2.5	0.16	ASTM 4984
Ti-15V-3Cr-3Al-3Sn	0.05	0.05	0.015	0.25	0.13	ASTM B348
Ti-11.5Mo-6Zr-4.5Sn	0.03	0.10	0.020	0.35	0.18	Ref. 22
Ti-5Al-5V-5Mo-3Cr	0.05	0.10	0.015	0.50	0.18	Ref. 22
Ti-13V-11Cr-3Al	0.05	0.05	0.025	0.35	0.17	Ref. 22
Ti-8Mo-8V-2Fe-3Al	0.05	0.05	0.015	2.4	0.16	Ref. 22
Ti-13Nb-13Zr	0.05	0.08	0.009	0.25	0.15	ASTM F1713-43
Ti-15Mo	0.05	0.10	0.015	0.10	0.20	ASTM F2066-2008

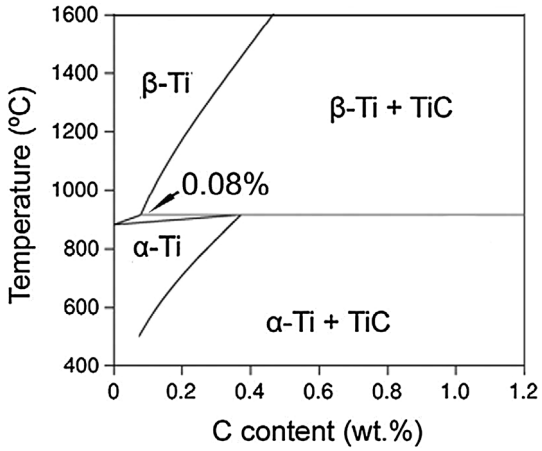

Fig. 1. Ti-C phase diagram up to 1.2 wt.% of carbon, predicted using Thermo-Calc Software 2008 and Ti alloys database V3 (TTTI3).[15] Reprinted from Ref. 15, p. 1015, with permission from Elsevier.

1.2 wt.% of C, predicted using Thermo-Calc Software 2008 (Thermo-Calc Software Inc., McMurray, PA) and Ti alloys database V3 (TTTI3). The formation of titanium carbide can lead to the following consequences: (I) raising chemical inhomogeneity and therefore resulting in reduced corrosion resistance; (II) introducing brittle ceramic phases into the microstructure and thus leading to reduced elongation and fatigue property; and (III) enhancing the overall Young's modulus due to the high modulus of titanium carbide itself and therefore widens the mismatch between the implant Ti material and human bones in terms of modulus.[14–16] These negative impacts on mechanical performance and corrosion resistance can be inferred from a variety of studies such as Refs. 17–19 as well as the results to be disclosed below for as-sintered Ti-Nb alloys. In the biological context, continuous titanium carbide coating may improve biocompatibility and osseointegration compared with uncoated Ti, but this is not expected to apply to discontinuous, impurity-induced grain boundary titanium carbide particles observed by several independent studies.[20,21]

To avoid the formation of titanium carbide (TiC_x), the carbon content in pure titanium should be limited to less than 0.08 wt.% (Fig. 1). This prediction has served as the theoretical basis for defining the carbon limit in most Ti alloys including many near β- and β-Ti alloys, while a reduced carbon limit, specified as 0.05 wt.%, has been used for some near β- and β-Ti alloys (with the exception of Ti-15V-3Cr-3Al-3Sn as a sheet alloy, whose carbon limit is set as 0.03 wt.%).[22] For biomedical β-Ti alloys such as Ti-13Nb-13Zr and Ti-15Mo listed in Table I, their carbon limit has simply followed the predicted value of (0.08–0.10) wt.% for pure Ti. In summary, the role of trace C in biomedical β-Ti alloys has not been adequately investigated compared with other common impurities (O, Fe, N, and H).

Recent studies on a few biomedical β-Ti alloys have shown that TiC_x particles can form in these alloys at carbon contents well below their respective limits set by the ASTM Standard Specifications.[15,16,23] This article reviews the recent progress in understanding the role of trace C in biomedical β-Ti alloys based on several detailed studies of trace C in Ti-Nb and Ti-Mo alloys. The precipitation mechanism of the TiC_x particles in these alloys is discussed based on the influence of Nb and Mo on the phase diagram and the change in the lattice parameter of the resulting β-Ti phase. The Ti-Nb and Ti-Mo systems are selected because Nb and Mo are two important alloying elements for biomedical β-Ti alloys. For instance, several successful biomedical β-Ti alloys have already been developed based on alloying with Nb and/or Mo Ti-13Nb-13Zr, Ti-35Nb-5Ta-7Zr, Ti-29Nb-13Ta-4.6Zr, Ti-24Nb-4Zr-8Sn, Ti-15Mo, and Ti-25Nb-2Mo-4Sn.[24–29] In fact, many of the aforementioned β-type Ti-Nb- and Ti-Mo-based alloys can be regarded as the second-generation biomedical Ti alloys which were developed to partially or fully replace the first-generation Ti biomaterials (e.g., CP-Ti and Ti-6Al-4V).

Table II. Impurity levels of the starting powders and as-sintered samples (wt.%)[16]

Material	C	O	N
Ti powder	0.00469	0.0744	0.0375
Nb powder	0.0152	0.221	0.0890
CP-Ti	0.0503	0.175	0.0628
Ti-10Nb	0.0562	0.203	0.0678
Ti-16Nb	0.0600	0.255	0.0525
Ti-22Nb	0.0589	0.225	0.0547

Reprinted from Ref. 16, p. 173, with permission from Elsevier.

CARBON IN Ti-Nb ALLOYS

Owing to their low elastic modulus and superior biocompatibility, Ti-Nb-based alloys are attracting increasing attention for biomedical applications.[30] Several studies have examined the role of carbon in these alloys. Hosoda et al.[31] have recently shown that an addition of (0.2–0.5) wt.% of carbon to a Ti-27 at.%Nb, i.e., Ti-41 wt.%Nb, alloy can refine the grain structure (the grain size decreased with increasing carbon concentration) because of the grain boundary pinning effect of the resulting TiC_x particles. In addition, the critical stress for slip increased as a result of the formation of TiC_x. However, the addition of such a level of carbon as an alloying element often risks embrittling the alloy also because of the formation of carbides. A notable exception is that reported by Li et al.,[32] who introduced more than 0.1 wt.% of C to a β-Ti alloy of Ti-25V-15Cr-2Al (wt.%) and achieved a dramatic increase in tensile elongation (from less than 2% to more than 20%). The reason was attributed to the formation of Ti_2C particles, which scavenged oxygen from the Ti matrix leading to much improved tensile ductility. However, the formation of Ti_2C carbides in other β-Ti alloys has consistently resulted in a substantial decrease in tensile elongation as will be shown below. Hence, it is uncommon to introduce extra carbon to β-Ti alloys. Rather, the carbon content should be strictly controlled in most cases.

A more recent study by Zhao et al.[16] has examined the influence of carbon as a impurity on the microstructure and mechanical properties of three Ti-Nb binary alloys (Ti-10Nb, Ti-16Nb, and Ti-22Nb, all in wt.%), processed by metal injection molding (MIM) and sintering. Gas-atomized Ti powder (<45 μm) and hydride/dehydride Nb powder (<110 μm) were used to fabricate the samples. Additionally, CP-Ti samples were fabricated by the same MIM process as a point of reference. After chemical and thermal debinding, all samples were sintered at 1500°C for 4 h. Table II lists the impurity levels of the starting powders and the as-sintered samples. Due to reactions with the residual polymeric binder during thermal debinding and sintering, the carbon content of the as-sintered samples increased by about (0.045–0.050) wt.% compared with the carbon content of the starting powders, but the total C content is still clearly below 0.08 wt.%. Acicular TiC_x particles were observed in all as-sintered Ti-Nb samples, while the as-sintered CP-Ti samples were free of the formation of carbides. Figure 2 shows the microstructures of the as-sintered CP-Ti and Ti-22Nb samples. Strip-shaped TiC_x particles were found residing on the grain boundaries of the as-sintered Ti-22Nb sample.

A detailed microstructural study of the as-sintered Ti-22Nb alloy was performed using transmission electron microscopy (TEM) as shown in Fig. 3, in order to better understand the nature of the TiC_x particles. The selected-area electron diffraction (SAED) pattern of the TiC_x particle revealed that the carbide phase exhibited a face-centered-cubic (fcc) structure with lattice parameter a = 4.3 Å. The extra diffraction maxima at various zone axes with much lower intensity suggests that the TiC_x particle should be *Fd3m*-Ti_2C, which is consistent with the titanium carbide (Ti_2C) identified in the Ti-25V-15Cr-2Al (wt.%) alloy.[32] However, it should be pointed out that the conditions under which Ti_2C, rather than TiC, forms in a β-Ti alloy remains to be an unanswered question. The following crystallographic relationship was identified between the Ti_2C particle and its surrounding body-centered-cubic (bcc) β-Ti matrix: $(11\bar{1})_{Ti_2C}//(110)_{\beta-Ti}$ and $[011]_{Ti_2C}//[001]_{\beta-Ti}$. Besides, reflections from hexagonal-close-packed (hcp) α-Ti were also observed in Fig. 3d. According to Sekimoto et al.,[33] a small amount of *Fd3m*-Ti_2C particles may have transformed into α-Ti in the β-Ti matrix. For example, the (111) plane of the *Fd3m*-Ti_2C could transform itself into the (0001) plane of α-Ti through sliding, with the stacking sequences changing from the ABCABC type in the former lattice to the ABAB type in the latter. In this case, the crystallographic relationship between α-Ti and *Fd3m*-Ti_2C will follow: $(111)_{Ti_2C}//(0001)_{\alpha-Ti}$.

To eradicate the influence of residual porosity on the mechanical properties, the as-sintered CP-Ti and Ti-Nb alloys were subjected to hot isostatic pressing (HIP). Table III lists the area fractions of

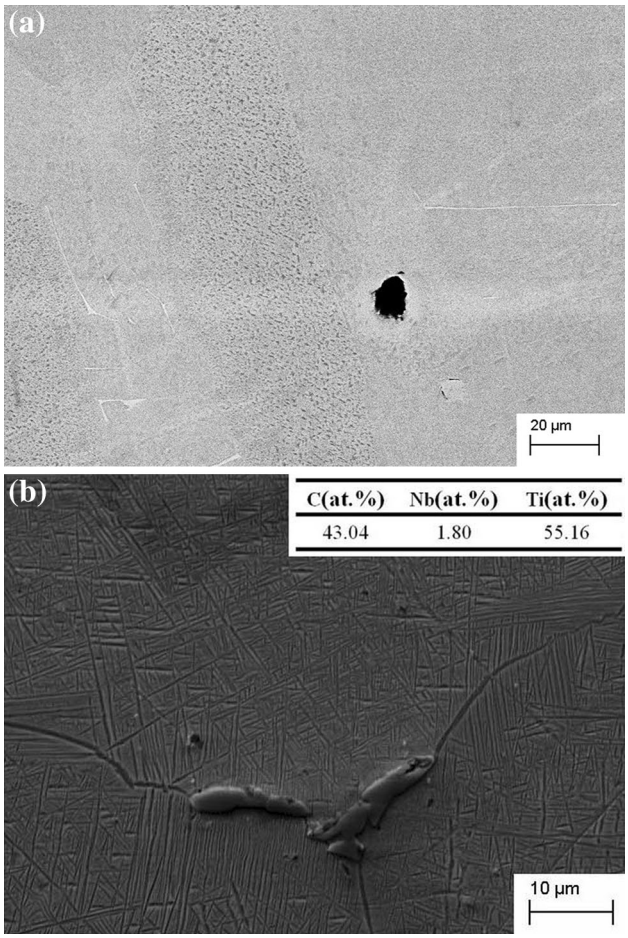

Fig. 2. Microstructures of MIM-processed and sintered (a) CP-Ti and (b) Ti-22Nb samples (SEM images). The inset in Fig. 2b shows the EDS results of carbide particles.

carbides and tensile properties of as-HIP CP-Ti and Ti-Nb samples. The amount of TiC_x particles showed a clear dependency on the Nb content. As a result, the tensile elongation of the as-HIP, pore-free Ti-Nb alloys decreased linearly with increasing Nb content (see Table III). However, the tensile strength showed the opposite trend, which can be attributed to the strengthening effect spawned by the carbide particles.

Figure 4 shows a longitudinal section of the fractured tensile specimen of the as-HIP Ti-22Nb alloy including part of the fracture surface profile. Microcracks were found to have initiated from the carbide particles. In addition, most carbide particles were fragmented showing cross-sectional microcracks perpendicular to the tensile direction. These observations explain the linear drop in tensile elongation with increasing Nb content, which corresponds to the nearly linear increase in the area fraction of carbides.

In addition to the MIM-processed Ti-Nb binary alloys, carbide particles were also observed in an MIM-processed and HIP Ti-24Nb-4Sn-8Zr (Ti-2448) alloy containing a super-low level of carbon (0.009 wt.%).[34] Similar to the as-HIP Ti-Nb alloys discussed previously, this as-HIP Ti-2448 alloy showed very low tensile elongation (approximately 1.8%), due to the formation of carbides with an area fraction of around 1.5%.

CARBON IN Ti-Mo ALLOYS

Mo is the most effective β stabilizer: An introduction of 8 wt.% of Mo is sufficient to retain the β-Ti phase quenched from the β field,[35] whereas it requires 22 wt.% of Nb or 52 wt.% of Ta to stabilize the β-phase. ASTM F 2066-2008 defined the maximum carbon limit for wrought Ti-15Mo as 0.10 wt.% for surgical implant applications. However, TiC_x particles were observed in Ti-15Mo alloy samples containing just 0.032 wt.% of C.[15] The Ti-15Mo alloy was fabricated by uniaxial cold compaction of an mixture of titanium hydride (TiH_2) powder (99.5% purity, 95–106 μm) and elemental Mo powder (99.5% purity, <63 μm), followed by sintering at 1350°C for 2 h. Figure 5a shows a scanning electron microscopy (SEM) image of the primary α-Ti (designated as α_p-Ti), β-Ti matrix, and carbide particles in the as-sintered Ti-15Mo alloy. The grain boundary TiC_x particles exhibited a similar strip-like shape as observed in the MIM-processed Ti-Nb alloys. Figure 5b presents the SAED patterns of the TiC_x particles and the adjacent β-Ti matrix. The TiC_x particles in the as-sintered Ti-15Mo alloy exhibited the structure of $Fd3m$-Ti_2C with lattice parameter a = 4.29 Å, which is similar to the Ti_2C formed in the MIM-processed Ti-Nb alloys and those reported in Ti-25V-15Cr-2Al (wt.%) alloy.[32] Semi-coherent orientation relationships were identified between the carbide particles and the β-Ti matrix, and one of them is $(11\bar{1})_{Ti_2C}//(110)_{\beta-Ti}$ and $[112]_{Ti_2C}//[113]_{\beta-Ti}$.

TITANIUM CARBIDE PRECIPITATION MECHANISM IN β-Ti ALLOYS

As shown above, acicular TiC_x particles were observed in β-Ti alloys with carbon contents clearly below the critical carbon limit predicted for pure Ti (0.08 wt.%). Also, it has been found that the amount of carbides increases with increasing concentration of the β-stabilizers (Table III). It is thus necessary to assess the carbon solubility in Ti alloys containing β-stabilizers.

Figure 6 shows the Thermo-Calc predictions of the pseudo-binary (Ti-Nb)-C phase diagram with Nb contents of 10 wt.%, 16 wt.%, and 22 wt.%. There is a notable decrease in carbon solubility with increasing Nb content. The carbon limits in the β-(Ti-Nb) phase in the Ti-10Nb, Ti-16Nb, and Ti-22Nb alloys are 0.051 wt.% at 812°C, 0.036 wt.% at 718°C, and 0.021 wt.% at 735°C, respectively.

The precipitation mechanism of TiC_x particles can be understood using the pseudo-binary (Ti-Nb)-C phase diagrams. At the sintering temperature of

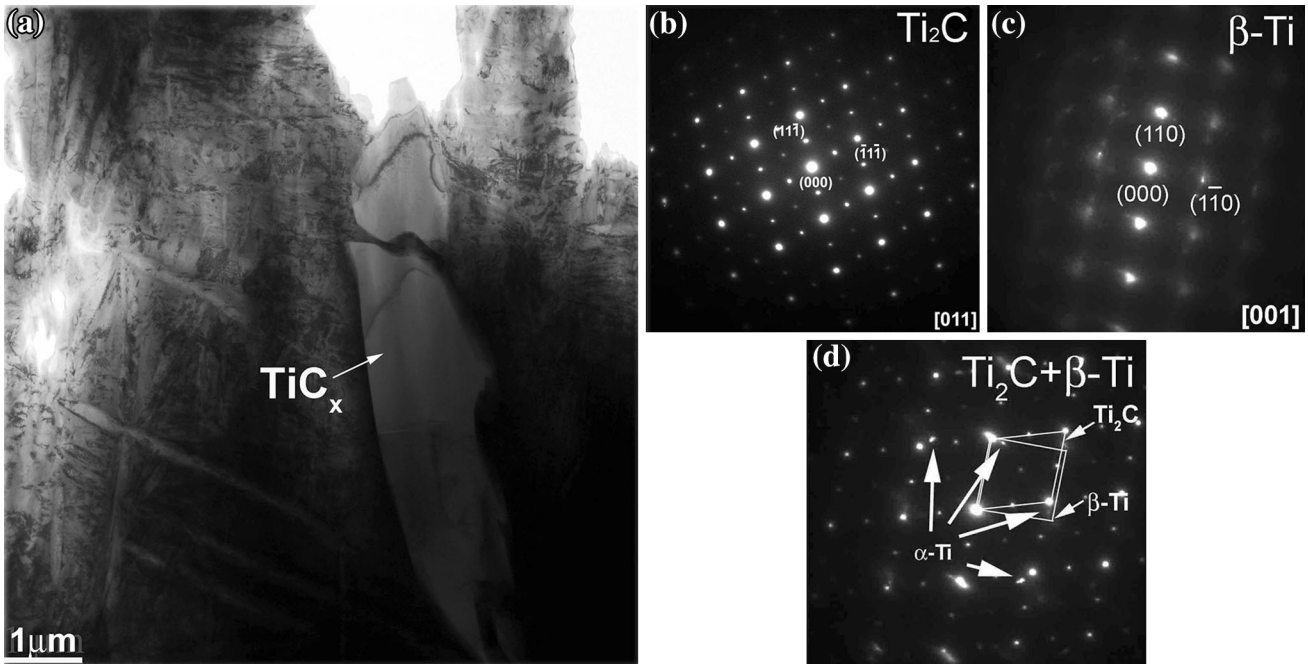

Fig. 3. TEM micrograph and SAED patterns of the as-sintered Ti-22Nb alloy: (a) the bright-field image; (b) a SAED pattern showing Ti_2C reflections from [011]; (c) a SAED pattern showing reflections of the matrix around the Ti_2C precipitate, the pattern was found to be β-Ti reflections from [001]; and (d) a SAED pattern showing both Ti_2C and β-Ti reflections as well as several diffraction spots from α-Ti.[16] Reprinted from Ref. 16, p. 176, with permission from Elsevier.

Table III. Area fraction of carbides and tensile properties of as-HIP CP-Ti and Ti-Nb alloys[16]

Composition	Carbide area fraction (%)	Ultimate tensile strength (MPa)	Elongation (%)	Young's modulus (GPa)
CP-Ti	0	586 ± 1.0	24.2 ± 2.2	116 ± 2.3
Ti-10Nb	0.51 ± 0.08	708 ± 4.5	9.63 ± 1.1	90.1 ± 6.1
Ti-16Nb	0.96 ± 0.15	739 ± 27	4.96 ± 0.31	82.2 ± 5.0
Ti-22Nb	1.87 ± 0.61	838 ± 14	1.30 ± 0.41	75.6 ± 7.6

Reprinted from Ref. 16, p. 179, with permission from Elsevier.

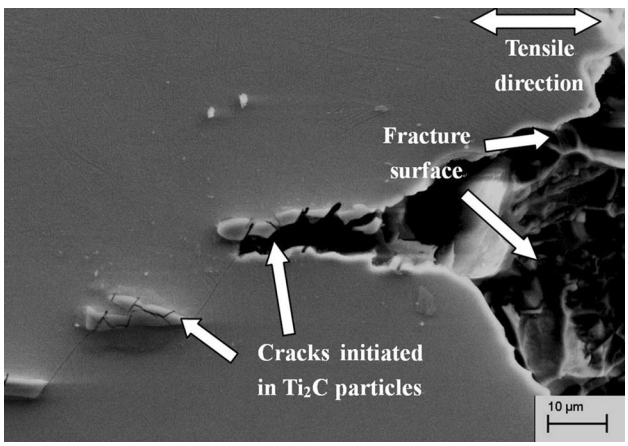

Fig. 4. SEM micrograph along the longitudinal section of a fractured as-HIP Ti-22Nb sample showing fragmented carbide particles and microcracks.

1500°C, the carbon solubility levels in Ti-10Nb, Ti-16Nb, and Ti-22Nb alloys are 0.307 wt.%, 0.278 wt.%, and 0.251 wt.%, respectively, compared with the total carbon content of (0.05–0.07) wt.% in each alloy (see Table II). Consequently, all the carbon should be in solid solution at the end of isothermal sintering at 1500°C for 4 h. During subsequent cooling, the solubility of carbon in β-Ti phase decreases with decreasing temperature, reaching 0.051 wt.% at 812°C for Ti-10Nb, 0.036 wt.% at 718°C for Ti-16Nb, and 0.021 wt.% at 735°C for Ti-22Nb. Precipitation of carbides is thus expected to occur during cooling. As the temperature further decreases, although the solubility of carbon actually increases to 0.161 wt.% at 723°C for Ti-10Nb, 0.117 wt.% at 678°C for Ti-16Nb, and 0.089 wt.% at 641°C for Ti-22Nb (see Fig. 6), because of the relatively low temperature, no dissolution of carbides is

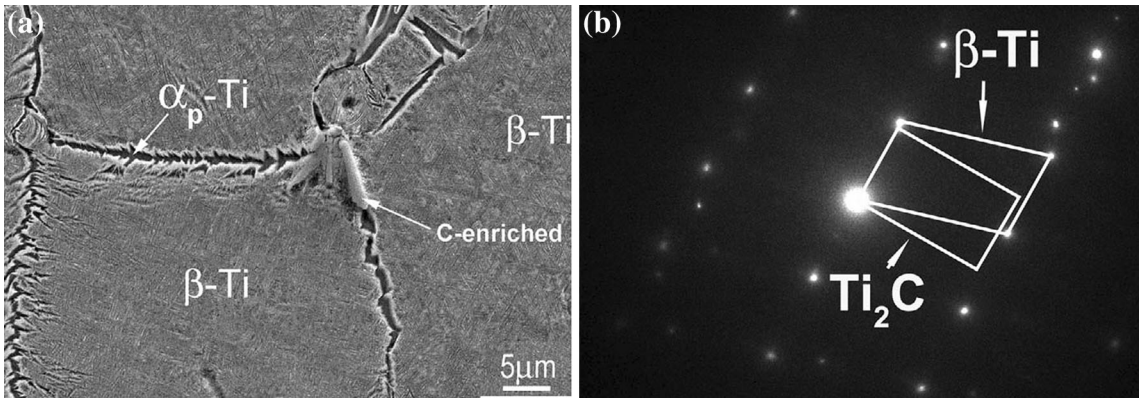

Fig. 5. (a) SEM image of the as-sintered Ti-15Mo alloy and (b) an overlap of the SAED patterns of the TiC_x particles and the adjacent β-Ti matrix.[15] Reprinted from Ref. 15, pp. 1015 and 1019, with permission from Elsevier.

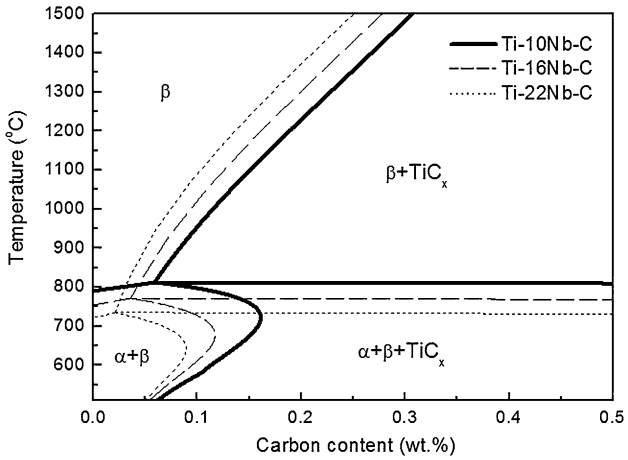

Fig. 6. Pseudo-binary phase diagrams of (Ti-10Nb)-C, (Ti-16Nb)-C, and (Ti-22Nb)-C up to 0.5 wt.% of carbon predicted using Thermo-Calc software.

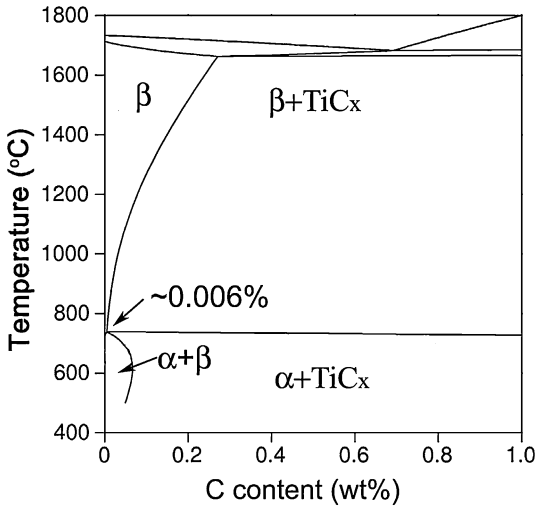

Fig. 7. Pseudo binary (Ti-15Mo)-C phase diagram up to 1.0 wt.% of C predicted using Thermo-Calc software.[15] Reprinted from Ref. 15, p. 1020, with permission from Elsevier.

expected. The precipitation of carbides thus mainly occurs during the first stage of cooling. Further precipitation during cooling below 500°C (see Fig. 2) is also possible.

Similar to the pseudo-binary (Ti-Nb)-C phase diagrams shown in Fig. 6, the pseudo-binary (Ti-15Mo)-C phase diagram constructed using Thermo-Calc, shown in Fig. 7, also revealed a significant decrease of carbon solubility in β-Ti because of the introduction of the 15 wt.% of Mo. The carbon solubility in the β-Ti phase of the Ti-15Mo alloy is 0.006 wt.% at 735°C compared to 0.08 wt.% of C without Mo (see Fig. 1). This critical carbon level (0.006 wt.%) is far below the actual carbon content of the MIM-processed Ti-15Mo alloy, which is about 0.05–0.07 wt.%.[15] As a consequence, there was noticeable formation of carbides in the Ti-15Mo alloy despite the presence of just a trace level of carbon (0.05–0.07) wt.%.

The above observations also occur to Ti-V based β-Ti alloys, although V is not preferred for biomedical applications.[36] Figure 8 shows the pseudo-binary (Ti-15V)-C phase diagram up to 0.5 wt.% of C predicted using Thermo-Calc software. The solubility of C in β-Ti decreased from 0.08 wt.% without V (see Fig. 1) to just 0.0113 wt.% (see Fig. 8) at the indicated temperature. Consequently, grain boundary carbides are readily observable in the aged MIM-processed Ti-15V-3Al-3Sn-3Cr (Ti-15333) alloy, which contained only 0.046 wt.% of C (see Fig. 9).

The significant impact of the β-stabilizers, particularly Nb and Mo (also including V), on the carbon solubility in the β-Ti matrix can also be understood according to the change of the lattice parameter of β-Ti after adding these alloying elements. For instance, Severino Martins and Grandini[37] have found that the addition of Mo reduces the lattice parameter of the β-phase in pure Ti. At room temperature, the lattice parameter of pure β-Ti is 3.31 Å (JCPDS PDF database # 44-1288), whereas that of β-(Ti-15Mo) is 3.26 Å.[37] Similarly,

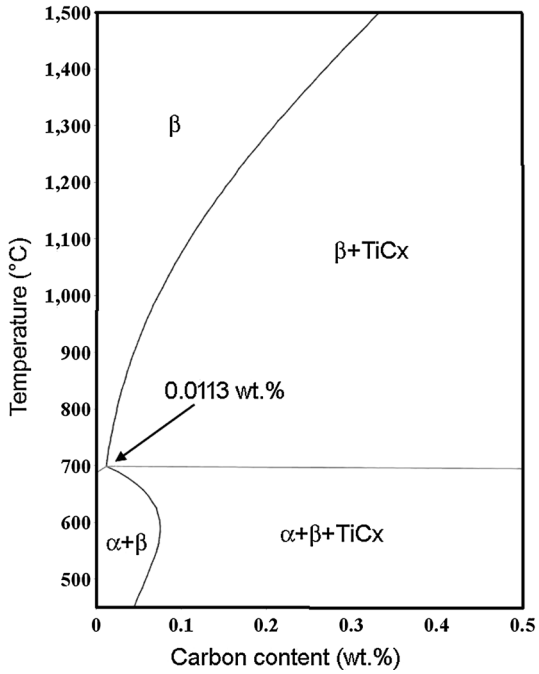

Fig. 8. Pseudo binary (Ti-15V)-C phase diagram up to 0.5 wt.% of carbon predicted using Thermo-Calc software.

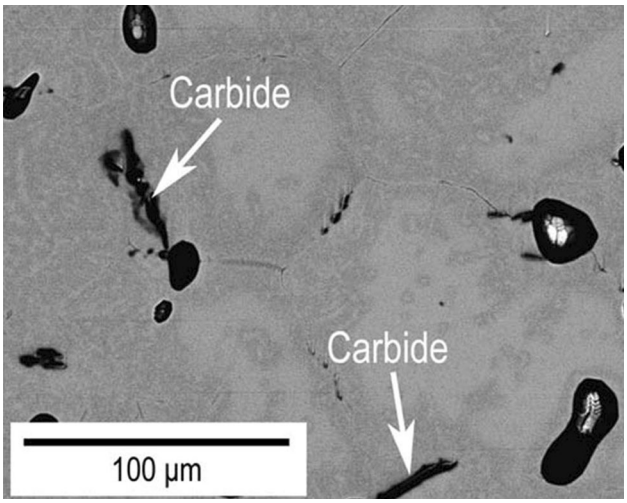

Fig. 9. Microstructure of aged MIM-processed Ti-15V-3Al-3Sn-3Cr (Ti-15333) alloy. Samples were sintered at 1400°C for 2 h after MIM and then aged at 500°C for 12 h. The C, O, and N contents were about 0.046 wt.%, 0.21 wt.%, and 0.024 wt.%, respectively. Energy-dispersive spectroscopy (EDS) revealed that the grain boundary precipitates are TiC_x particles despite the very low carbon content (0.046 wt.%).

the lattice parameter of β-(Ti-22Nb) was determined to be 3.277 Å by high-energy x-ray diffraction measurements.[38] In the β-Ti lattice, the addition of β-stabilizers such as Mo and Nb reduces the tetrahedral vacancy space and therefore leads to a significant decrease of the carbon solubility, favoring the formation of TiC_x particles.

SUMMARY AND FUTURE WORK

This work aims at understanding the influence of trace carbon (≤0.08 wt.%) on the microstructure and mechanical properties of β-Ti alloys. Acicular TiC_x precipitates have been observed in a variety of β-Ti alloys, such as Ti-Nb and Ti-Mo alloys. These carbides are usually distributed along grain boundaries. The TiC_x particles exhibit an fcc structure with lattice parameter of about a = 4.3 Å, and they have been determined to be $Fd3m$-Ti_2C. The carbide particles and the adjacent matrix show a crystallographic relationship, which can be described as $(111)_{Ti_2C}//(0001)_{\alpha-Ti}//(110)_{\beta-Ti}$. These grain-boundary Ti_2C particles have proved to be highly detrimental to the tensile ductility of these alloys and are expected to be detrimental to the fatigue property and corrosion resistance of these alloys because of the microstructural homogeneity.

The precipitation of the Ti_2C carbides results from the significantly reduced carbon solubility in the β-Ti matrix after introducing the β-stabilizing elements. The addition of these elements decreases the lattice parameter of the bcc β-Ti matrix, leading to less tetrahedral vacancy space. Thus, less carbon can stay in the matrix as interstitial atoms, which leads to the precipitation of carbides.

Because of their negative impacts on microstructural homogeneity and mechanical property, it is necessary to avoid the formation of TiC_x precipitates in biomedical β-Ti alloys. However, this implies that the carbon content in some biomedical β-Ti alloys should be controlled to be less than 0.006 wt.%. This may prove to be impractical or too costly to do so. A potential remedy is to apply a proper heat-treatment process, followed by quenching. This needs to be explored in the future for these alloys. In addition, it would be useful to understand why Ti_2C rather than TiC forms in all these β-Ti alloys.

ACKNOWLEDGEMENTS

This research was funded by Young Teacher Growth Plan (File No. 531107040850). M. Qian acknowledges the financial support of the Australian Research Council (ARC) through ARC LP140100607. D. Zhao and T. Ebel are grateful to Prof. Florian Pyczak and Prof. Regine Willumeit from Helmholtz-Zentrum Geesthacht for the assistance and input. Dr. Shenglu Lu of The University of Queensland is acknowledged for the calculations of the pseudo-binary (Ti-15V)-C phase diagram.

REFERENCES

1. M. Niinomi, M. Nakai, and J. Hieda, *Acta Biomater.* 8, 3888 (2012).
2. L.C. Zhang, D. Klemm, J. Eckert, Y.L. Hao, and T.B. Sercombe, *Scripta Mater.* 65, 21 (2011).
3. M. Geetha, A.K. Singh, R. Asokamani, and A.K. Gogia, *Prog. Mater. Sci.* 54, 397 (2009).
4. T. Saito, T. Furuta, J.-H. Hwang, S. Kuramoto, K. Nishino, N. Suzuki, R. Chen, A. Yamada, K. Ito, and Y. Seno, *Science* 300, 464 (2003).

5. W.F. Ho, C.P. Ju, and J.H. Chern Lin, *Biomaterials* 20, 2115 (1999).
6. D. Zhao, K. Chang, T. Ebel, H. Nie, R. Willumeit, and F. Pyczak, *J. Alloys Compd.* 640, 393 (2015).
7. T. Ahmed and H.J. Rack, *J. Mater. Sci.* 31, 4267 (1996).
8. Y.L. Hao, S.J. Li, S.Y. Sun, and R. Yang, *Mater. Sci. Eng. A* 441, 112 (2006).
9. L.-J. Xu, S.-L. Xiao, J. Tian, and Y.-Y. Chen, *Trans. Nonferrous Met. Soc. China* 23, 692 (2013).
10. K. Miura, N. Yamada, S. Hanada, T.-K. Jung, and E. Itoi, *Acta Biomater.* 7, 2320 (2011).
11. M. Yan, M.S. Dargusch, T. Ebel, and M. Qian, *Acta Mater.* 68, 196 (2014).
12. M. Nakai, M. Niinomi, T. Akahori, H. Tsutsumi, and M. Ogawa, *Mater. Trans.* 50, 2716 (2009).
13. M. Yan, M. Qian, T.T. Song, M.S. Dargusch, and X.S. Wei, *MRS Commun.* 4, 183 (2014).
14. H. Choe, S. Abkowitz, S.M. Abkowitz, and D.C. Dunand, *Mater. Sci. Eng. A* 485, 703 (2008).
15. M. Yan, M. Qian, C. Kong, and M.S. Dargusch, *Acta Biomater.* 10, 1014 (2014).
16. D. Zhao, K. Chang, T. Ebel, M. Qian, R. Willumeit, M. Yan, and F. Pyczak, *J. Mech. Behav. Biomed. Mater.* 28, 171 (2013).
17. R. Banoth, R. Sarkar, A. Bhattacharjee, T.K. Nandy, and G.V.S. Nageswara, Rao. *Mater. Des.* 67, 50 (2015).
18. A. Shanaghi, P.K. Chu, A.R. Sabour Rouhaghdam, R. Xu, and T. Hu, *Surf. Coat. Technol.* 229, 151 (2013).
19. Y.-J. Kim, H. Chung, and S.-J.L. Kang, *Mater. Sci. Eng. A* 333, 343 (2002).
20. M. Brama, N. Rhodes, J. Hunt, A. Ricci, R. Teghil, S. Migliaccio, C.D. Rocca, S. Leccisotti, A. Lioi, M. Scandurra, G. De Maria, D. Ferro, F. Pu, G. Panzini, L. Politi, and R. Scandurra, *Biomaterials* 28, 595 (2007).
21. G. Longo, M. Girasole, G. Pompeo, A. Cricenti, C. Misiano, A. Acclavio, A.C. Tizzoni, L. Mazzola, P. Santini, L. Politi, and R. Scandurra, *Surf. Coat. Technol.* 204, 2605 (2010).
22. J. Matthew and J. Donachie, *Titanium: A Technical Guide* (ASM International: Materials Park, 2000).
23. D. Zhao, K. Chang, T. Ebel, M. Qian, R. Willumeit, M. Yan, and F. Pyczak, *Powder Metall.* 57, 2 (2014).
24. K.S. Suresh, N.P. Gurao, S. Singh, S. Suwas, K. Chattopadhyay, S.V. Zherebtsov, and G.A. Salishchev, *Mater. Charact.* 82, 73 (2013).
25. C.R.M. Afonso, P.L. Ferrandini, A.J. Ramirez, and R. Caram, *Acta Biomater.* 6, 1625 (2010).
26. M. Niinomi, *Biomaterials* 24, 2673 (2003).
27. Y. Yang, P. Castany, M. Cornen, F. Prima, S.J. Li, Y.L. Hao, and T. Gloriant, *Acta Mater.* 88, 25 (2015).
28. A. Kazek-Kęsik, M. Krok-Borkowicz, E. Pamuła, and W. Simka, *Mater. Sci. Eng. C* 43, 172 (2014).
29. S. Guo, Q. Meng, G. Liao, L. Hu, and X. Zhao, *Prog. Nat. Sci.* 23, 174 (2013).
30. A. Terayama, N. Fuyama, Y. Yamashita, I. Ishizaki, and H. Kyogoku, *J. Alloys Compd.* 577, S408 (2013).
31. H. Hosoda, Y. Horiuchi, T. Inamura, K. Wakashima, H.Y. Kim, and S. Miyazaki, *Mater. Sci. Forum* 638–642, 2046 (2010).
32. Y.G. Li, P.A. Blenkinsop, M.H. Loretto, D. Rugg, and W. Voice, *Acta Mater.* 47, 2889 (1999).
33. W. Sekimoto, H. Tsuda, and S. Mori, *Mater. Trans.* 53, 1405 (2012).
34. F. Kafkas and T. Ebel, *J. Alloys Compd.* 617, 359 (2014).
35. N.T.C. Oliveira, G. Aleixo, R. Caram, and A.C. Guastaldi, *Mater. Sci. Eng. A* 452–453, 727 (2007).
36. H.M. Silva, S.G. Schneider, and C.M. Neto, *Mater. Sci. Eng. C* 24, 679 (2004).
37. J.R. Severino Martins and C.R. Grandini, *J. Appl. Phys.* 111, 083535 (2012).
38. D. Zhao (Dr.-Ing. Doctor Thesis, Brandenburgische Technische Universität Cottbus-Senftenberg, 2014).
39. M. Semlitsch, *Clin. Mater.* 2, 1 (1987).